www.lajss.org
Latin American Journal of Solids and Structures 5 (2008) 47–73

Modal analysis of orthotropic composite floors slabs with profiled steel decks

A. V. de A. Mello[a], J. G. S. da Silva[b,*], P. C. G. da S. Vellasco[c], S. A. L. de Andrade[c,a] and L. R. O. de Lima[c]

[a]Civil Engineering Department, Pontifical Catholic University of Rio de Janeiro, PUC-Rio, Brazil
[b]Mechanical Engineering Department, State University of Rio de Janeiro, UERJ, Brazil
[c]Structural Engineering Department, State University of Rio de Janeiro, UERJ, Brazil

Abstract

When a composite floor system incorporates a profile steel deck slab, the slab isotropy assumption may be questionable. One of the most commonly used solutions to better represent the composite floor is to consider an orthotropic system where the major direction is parallel to the slab deck ribs axis. The main objective of this paper is to investigate the orthotropic solution for the composite slabs. The investigation was focused on the computational modelling of the dynamical behaviour of commonly used composite floors with profile steel decks. The composite floor studied in this work, spanning 43.7m by 14.0m, is currently used for gymnastics. The investigated structural system dynamical response, obtained from finite element method isotropic and orthotropic simulations, was compared to experimental evidence. The current investigation has also considered three fundamental aspects of the dynamical composite floor response i.e.: boundary condition effects, the steel profile deck contribution and the composite floor neutral axes location on the global structural system response. A subsequent parametric analysis was also performed to further verify the computational models accuracy. These models results were also compared to calculated and measured natural frequencies of a full-scale composite floor.

Keywords: vibration, dynamical analysis, composite structures, orthotropic composite floors, steel deck, parametric study, serviceability, human walking and dynamic structural design.

1 Introduction

Structural designers aiming to develop minimum cost solutions could be faced with the production of slender structural solutions that could modify the ultimate and serviceability limit states that govern their structural behaviour. These facts could lead to a considerable increase in the problems related to unwanted floor vibrations. This phenomenon is becoming very frequent in a wide range of structures subjected to dynamical actions. These load actions are generally caused by human activities such as: sporting events, dance or even gymnastics, as referred namely by

*Corresp. author email: jgss@uerj.br
Received 22 Aug 2007; In revised form 13 Feb 2008

Bachmann & Ammann [2], Chen [3], Mello [6], Mello et al. [7], Murray et al. [8], Silva et al. [4], Silva et al. [5].

The presence of undesirable vibrations in building floors can be attribute to the fact that a significant number of structural engineers disregard, or even do not know how to incorporate the dynamical actions in the structural analysis. This procedure limits current structural designs to a simple static analysis that can, in extreme cases, demand a structure redesign or even a structure retrofitting. These facts enlighten the main objective of the current investigation: to evaluate the influence of the orthotrophy in the dynamical structural response of commonly used composite structural systems as referred by Silva et al. [4, 5].

When a composite floor incorporates a steel deck, the isotropy of the structural system is a hypothesis that can be at least considered questionable. One of the most commonly used solutions to better represent the composite floor is to consider it an orthotropic system where the major direction is parallel to the steel deck ribs span.

A usual design assumption considers the major direction stiffness as the addition of the portion related to the concrete slab above the steel deck ribs plus an extra term that incorporates an "effective width" based on the ratio of concrete area present in the ribs over the overall area (ribs + voids). In the minor direction, only the first part is considered i.e. the concrete cover slab, above the concrete slab ribs. This simple hypothesis can be easily incorporated to any design model and the results strongly depend on the steel deck geometry.

One of the main outcomes of the present investigation comes from the possible differences arising from the isotropic and orthotropic modelling based on the natural frequencies and associated vibration modes of a real composite floor. These parameters were also compared to the measured experimental values [10]. With these results in hand, the study followed with an extensive parametric study considering boundary condition effects, steel deck geometry and the inclusion of the actual beam-to column joint stiffness.

2 Composite structures

Composite steel-concrete structures are widely used in modern bridge and building construction. A composite member is formed when a steel component, such as an I-section beam, is associated to a concrete element, such as a floor slab or bridge deck. In such a composite T-beam, as presented in Fig. 1, the comparatively high load capacity of the concrete in compression complements the high strength of the steel in tension, [9].

The fact that each material, steel and concrete, is used to take advantage of its best attributes makes composite steel-concrete construction very efficient and economical. However the real attraction of composite construction is based on having an efficient steel to concrete connection and that this transfer of forces provides composite members their unique behaviour, [9]. Shear connectors like stud bolts, channel sections or perfobond plates are currently used to perform this task.

.

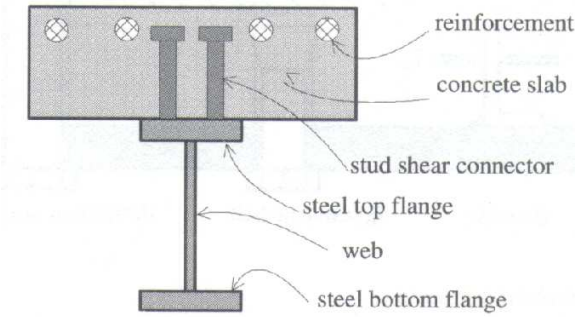

Figure 1: Composite T-beam.

Nowadays, most of the modern floor systems in buildings use a concrete slab with a cold formed profiled steel sheeting element (0.8mm thickness) as shown in Fig. 2. This is a special form of composite member where the composite action is achieved by embossments in the sheeting, as presented in Fig. 2, and by some chemical bonding between the concrete and steel sheeting, [9].

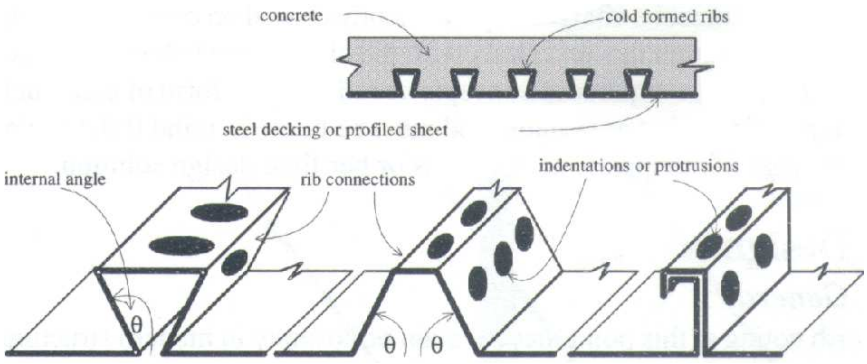

Figure 2: Composite profiled slabs [9].

When the steel component acts compositely with a concrete component, the cross-sectional shape of the composite slab, to be used in the structural analysis, depends on the relative direction of the span of the ribs of the concrete slab to the span of the steel component [4].

The composite floor analysed in this paper presents a cross-section in which the profile ribs span are in the same direction as the composite beam, as shown in Fig. 3, where (b_{eff})l and (b_{eff})r are the effective widths on the left and right of the steel component, h_{solid} is the height of the solid part of the concrete slab component, h_{rib} is the height of the rib, A_{rib} is the area of an individual rib, A_{void} is the area of an individual void between the ribs and θ=0^o, where θ

is the angle in degrees between the direction of the ribs span and the composite beam span, as presented in Fig. 4.

The structural system cross-section can be analysed as illustrated in Fig. 3, where the area of the haunch is equal to the areas of the individual ribs ΣA_{rib} over the effective width w_{eff} of the section. When θ=90^o the ribs are transverse to the direction of the span of the composite beam and the weakest cross-section in the structural analysis is used, as shown in Fig. 5.

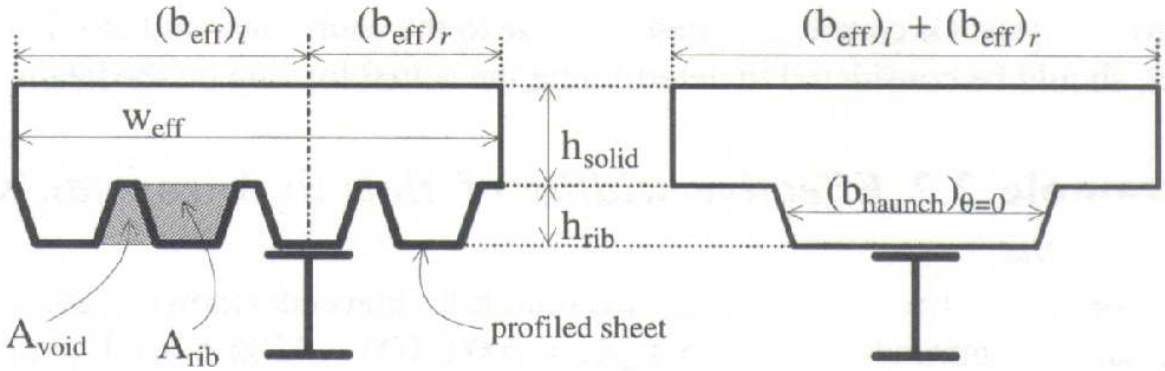

Figure 3: Longitudinal ribs ($\theta = 0^o$) [9].

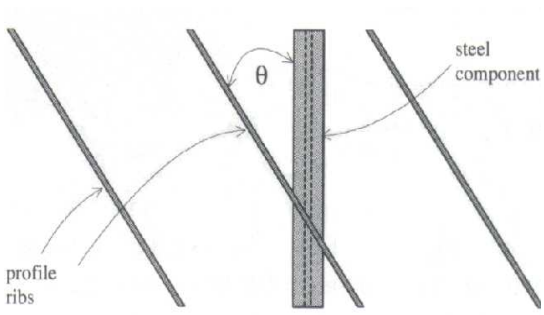

Figure 4: Oblique ribs ($\theta \neq 0^o$) [9].

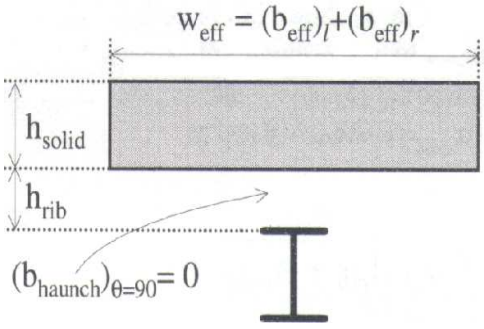

Figure 5: Transverse ribs ($\theta = 90^o$) [9].

3 Modelling of the dynamical behaviour

The computational models developed in the present investigation to proper represent the dynamical response of composite floor systems covered four distinct cases. These specific situations highlights a study made to investigate the influence of several parameters on the composite floor

dynamical response like: boundary conditions adopted in modelling, composite system neutral axis location, steel deck geometry and the actual stiffness provided by the beam to-columns joints.

These facts motivated the conception of four different models. The first structural model considers the composite floor systems as simply supported. The second structural model considers the composite floor system with rigid supports only located at the four floor corners while the other supports are still considered as simply supported. The third structural model considers all the supports as being rigid. In these three models the extra stiffness provided by the joints was not considered.

Finally the fourth model considered the extra stiffness provided by the steel joints. The effects of the floors above and below the studied composite structural system were taken into account in this model by considering simply supported 5m length columns.

It is also important to observe that the study concerning the variation of the composite neutral axis position over the system dynamical response was only made on the first structural model that considers the composite floor system as simply supported. Five different locations for the composite system neutral axis were investigated as depicted in Fig. 6.

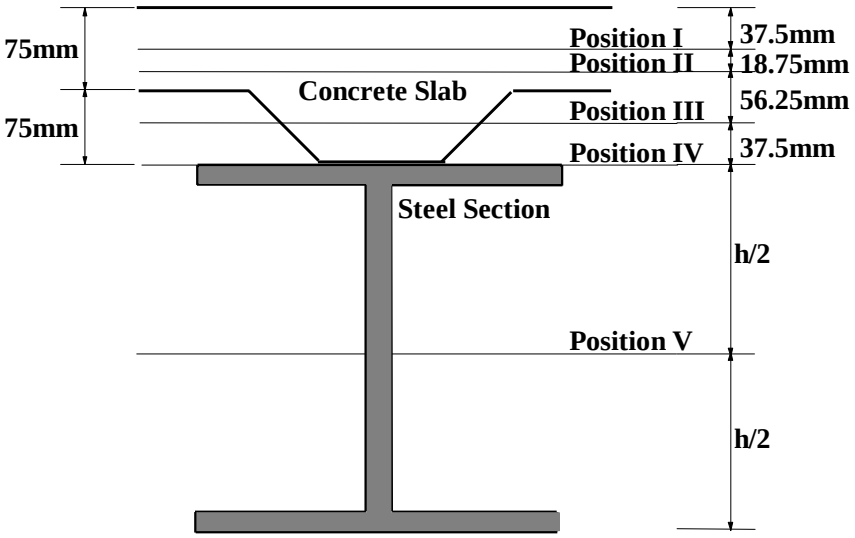

Figure 6: Neutral axis position variation along the system composite section height.

4 Structural system

The composite floor studied in the present paper is shown in Fig. 7. It spans 14.0m and is 43.7m wide, with an average distance between girder centre lines of 7.8m, and is currently used for gymnastics [10]. The structural system is made of composite girders. The 150mm

thick composite slab uses a steel deck with the following geometrical characteristics: 0.80mm thickness, and 75mm flute height, Fig. 8. The steel sections used were welded wide flanges (WWF) of 300MPa yield stress steel grade. The isotropic and orthotropic systems adopted a 205 GPa Young's modulus for the steel beams and deck.

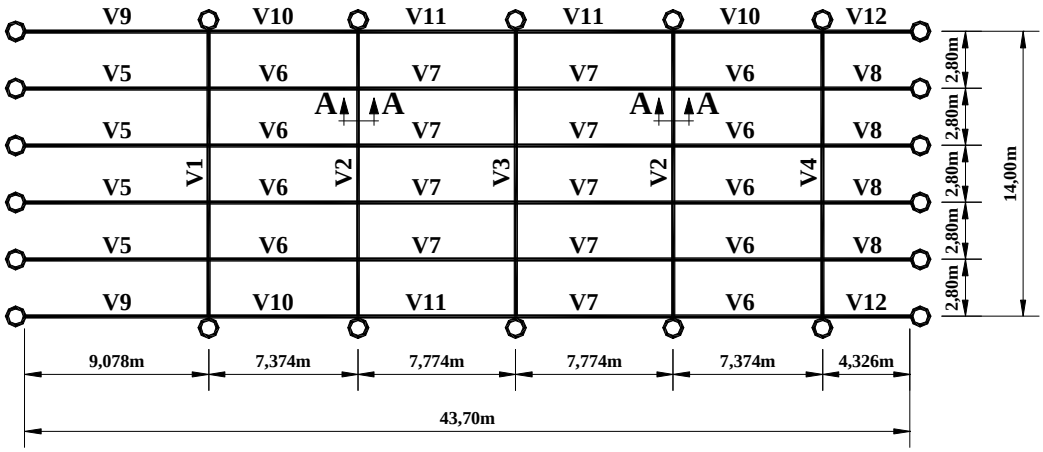

Figure 7: The structural model.

The concrete slab has a 20MPa specified compression strength and a 23.5 GPa Young's modulus [10]. However, according to Murray et al. [8], in such situations, where the composite slab is submitted to dynamic excitations, the concrete becomes stiffer than when it is submitted to pure static loads. Due to this fact, according to the authors a 35% increase in the conventional concrete Young's modulus used in the isotropic system is suggested. The structure permanent and live load were equal to 3.5kN/m^2 and 2kN/m^2.

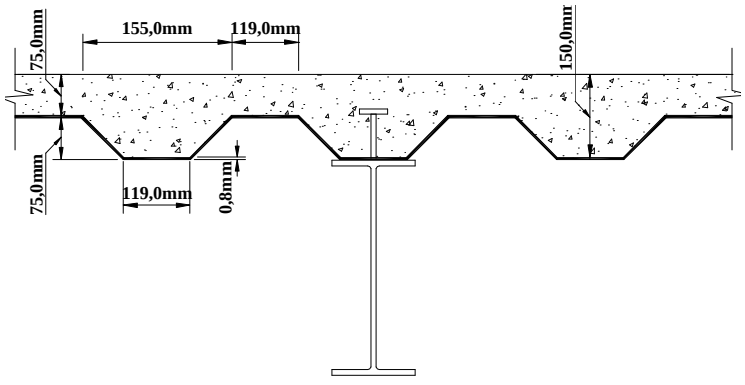

Figure 8: Typical composite slab cross-section: Section AA.

Tab. 1 depicts the geometrical characteristics of all the steel sections used in the structural

model, presented in Fig. 7 and 8. It is important to emphasize that there was a haunch present in the extreme spans of V1 to V4 girders. The minimum height of the steel sections near the supports was equal to 460.0mm, \cite{10}. The fourth model (that considered the extra stiffness provided by the beam to-columns joints) accounted for the 5m length columns made of a WWF 300 x 62 steel section with the geometrical characteristics presented in Tab. 1.

Table 1: Geometrical characteristics of the beam and column steel sections (mm).

Beams	Height (mm)	Flange Width (mm)	Thicknesses (mm)		
			Top Flange	Bottom Flange	Web
V1 to V4	1400	350	12.5	12.5	12.5
V5	700	200	8.0	8.0	8.0
V6 and V7	600	150	6.3	6.3	6.3
V8 and V12	250	130	6.3	6.3	4.75
V9	400	200	6.3	6.3	4.75
V10 and V11	400	150	6.3	6.3	4.75
Columns	Height (mm)	Flange Width (mm)	Thicknesses (mm)		
			Top Flange	Bottom Flange	Web
C 300 x 62	300	300	9.5	9.5	8.0

5 Computational model

The proposed computational model, developed for the composite slab dynamic analysis, adopted the usual mesh refinement techniques present in finite element method simulations implemented in the ANSYS program [1]. In the developed finite element model, floor steel girders are represented by three-dimensional beam elements, where flexural and torsion effects are considered. The composite slab is represented by a regular mesh of shell finite elements.

The combined actions of floor slab and steel beams were considered in the present investigation. The eccentricities of the floor slab and the steel beams were considered and significantly increases the composite floor stiffness. The computational model was developed taking into account this effect associated to the eccentricities of the floor slab and the steel beams. The ANSYS program has provided all the procedures related to the locations of the neutral axes of the effective widths of the plates using basic concepts of structural analysis. When a composite floor incorporates a steel deck, the isotropy of the structural system is, at least, a questionable hypothesis. One of the most commonly used solutions to better represent the composite floor is to consider it as an orthotropic model [6, 9].

In this paper, the major direction was considered parallel to the span of the slab ribs, as

presented in Fig. 3. The proposed computational model considers the major direction inertia as the addition of the part related to the concrete slab above the steel deck ribs plus an extra term that incorporates an effective width based on the ratio of concrete area present in the ribs over the overall area (ribs + voids). The minor direction only considers the first part i.e. the concrete slab above the concrete slab ribs, the so-called cover slab, as shown in Fig. 5.

In order to emulate the orthotropic system, different longitudinal and transverse Young's modulus, as well as Poisson ratios, for the concrete slab were used in the major/minor concrete slab plane directions, as well as in a direction perpendicular to this plane, according to the system orthotropic inertia characteristics. These values were calculated based on the simple, but effective, idea of modifying the longitudinal Young's modulus. Since the concrete inertia was kept constant in both directions to simplify the model geometry, the Young's modulus, in the direction parallel to the deck ribs, was increased. This was made to compensate for the extra area, and consequently, inertia provided by the concrete present in the deck ribs. With these results in hand, the transverse Young's modulus, as well as the Poisson ratios, were also re-evaluated. This was made accordingly to simple elasticity formulae for orthotropic materials. The increase in stiffness/resistance provided by the profiled steel sheet was not considered in the computational model.

The final computational model used 3366 nodes, 726 three-dimensional beam elements, BEAM44, and 3264 shell elements, SHELL63 [1], leading to a numerical model with 18012 degrees of freedom. The BEAM44 rigid offset capability, [1], was explored to incorporate, in the structural model, the combined floor beam section eccentricity due to the steel deck.

6 Modal analysis: natural frequencies and vibration modes

The composite floor dynamic response was initially determined through an analysis of its natural frequencies and vibration modes for the four studied models. The results were obtained through an extensive parametric study based on finite element simulations made with the already referred ANSYS program [1]. The natural frequencies and vibration modes were obtained for each model to identify the most suitable model to represent the investigated composite floor system.

The four distinct computational models were studied aiming to investigate the influence of several parameters on the composite floor dynamical response like: boundary conditions adopted in modelling, composite system neutral axis location, steel deck geometry and the actual stiffness provided by the beam to-columns joints.

The first structural model considers the composite floor supports as simply supported. The second structural model considers the composite floor supports as rigid supports only at the four floor corners while the other supports are still considered as simply supported. The third structural model considers all the support as being rigid.

Finally the fourth model considered the extra stiffness provided by the beam to-columns joints. The effects of the floors above and below the investigated composite structural sys-

tem were taken into account in this model by considering simply supported five meters length columns. Tabs. 2 to 9 depict the composite floor natural frequencies (eigenvalues) while the associated vibration modes (eigenvectors) are presented in Figs. 9 to 14. It is important to stress that Tabs. 2 to 9 covers numerous steel deck geometries by varying the ratio between the area of an individual rib, A_{rib}, and the sum, A_T, of the areas of a void, A_{void}, plus the rib, A_{rib}, i.e. $A_T = A_{rib} + A_{void}$.

Tabs. 2 to 5 also considered the variation of the composite neutral axis position over the system dynamical response. Five different locations for the composite system neutral axis were investigated, as depicted in Fig. 6. Due to the space restrictions this paper only presents the results of the first structural model that considers the composite floor supports as simply supported. The second and third models used the second position of the composite neutral axis illustrated in Fig. 6. Tabs. 2 to 9 present the numerical results based on a comparison of the isotropic and orthotropic models, also quantitatively evaluating the relation between these two strategies.

7 Results analysis and discussion

7.1 Calibration with the experimental results

The numerical results depicted in Tabs. 2 to 5 (that included the composite system neutral axis variation) clearly indicated that the results of the first model fundamental frequency agrees with the experimental test frequency, f_{01}=9.50Hz, referred by Vecci et al. [10]. This fact is the first step for the validation of the numeric models here presented, as well as the results and conclusions obtained throughout this investigation.

However, it must be emphasized that, as soon as the boundary conditions change, the composite system vibration modes configurations are modified. Unfortunately, the other composite floor natural frequency values and the structural system experimental first vibration mode were not provided in reference [10] for further comparisons with the numerical simulations.

The results, depicted in Tab. 3, for first model where the beam to-columns joints were simulated by using simple supports f_{01}=10.18Hz, is higher than the experimental value f_{01}=9.50Hz [10]. This small difference, around 7%, can be probably explained by the fact that the actual composite system neutral axis is located in a position different from the location assumed in the numerical analysis.

It should also be observed that the fundamental frequency results depicted in Tabs. 7 to 9 also showed to be in agreement with the first natural frequency experimentally obtained, f_{01}=9.50Hz, [10]. This was due to the smaller influence of using rigid supports in key points of the second model, f_{01}=10.24Hz.

On the other hand, the fourth model that explicitly considered the columns produced a fundamental frequency equal to f_{01}=9.30Hz, leading to the best fit with the fundamental frequency measured experimentally, f_{01}=9.50Hz, [10].

Table 2: First structural model: First composite section neutral axis position.

Frequencies (Hz)	Isotropic Model f_{0i}(I)	Orthotropic Model ($A_{rib}/A_T = 0.5$) f_{0i}(O)	f_{0i} (O)/ f_{0i}(I)
f_{01}	10.941	10.360	0.947
f_{02}	11.023	10.434	0.947
f_{03}	11.407	10.821	0.949
f_{04}	12.061	11.497	0.953
f_{05}	12.403	11.898	0.959
f_{06}	13.213	12.678	0.960
Frequencies (Hz)	Isotropic Model f_{0i}(I)	Orthotropic Model ($A_{rib}/A_T = 0.6$) f_{0i}(O)	f_{0i} (O)/ f_{0i}(I)
f_{01}	10.941	10.353	0.946
f_{02}	11.023	10.427	0.946
f_{03}	11.407	10.812	0.948
f_{04}	12.061	11.486	0.952
f_{05}	12.403	11.884	0.958
f_{06}	13.213	12.660	0.958
Frequencies (Hz)	Isotropic Model f_{0i}(I)	Orthotropic Model ($A_{rib}/A_T = 0.7$) f_{0i}(O)	f_{0i} (O)/ f_{0i}(I)
f_{01}	10.941	10.322	0.943
f_{02}	11.023	10.393	0.943
f_{03}	11.407	10.773	0.944
f_{04}	12.061	11.434	0.948
f_{05}	12.403	11.815	0.953
f_{06}	13.213	12.586	0.953
Frequencies (Hz)	Isotropic Model f_{0i}(I)	Orthotropic Model ($A_{rib}/A_T = 0.8$) f_{0i}(O)	f_{0i} (O)/ f_{0i}(I)
f_{01}	10.941	10.285	0.940
f_{02}	11.023	10.355	0.939
f_{03}	11.407	10.728	0.940
f_{04}	12.061	11.375	0.943
f_{05}	12.403	11.735	0.946
f_{06}	13.213	12.500	0.946
Frequencies (Hz)	Isotropic Model f_{0i}(I)	Orthotropic Model ($A_{rib}/A_T = 0.9$) f_{0i}(O)	f_{0i} (O)/ f_{0i}(I)
f_{01}	10.941	10.240	0.936
f_{02}	11.023	10.309	0.935
f_{03}	11.407	10.675	0.936
f_{04}	12.061	11.303	0.937
f_{05}	12.403	11.640	0.938
f_{06}	13.213	12.396	0.938

Table 3: First structural model: Second composite section neutral axis position.

Frequencies (Hz)	Isotropic Model f_{0i}(I)	Orthotropic Model ($A_{rib}/A_T = 0.5$) f_{0i}(O)	f_{0i} (O)/ f_{0i}(I)
f_{01}	10.743	10.184	0.948
f_{02}	10.853	10.265	0.946
f_{03}	11.192	10.617	0.949
f_{04}	11.791	11.241	0.953
f_{05}	12.070	11.576	0.959
f_{06}	12.914	12.388	0.959
Frequencies (Hz)	Isotropic Model f_{0i}(I)	Orthotropic Model ($A_{rib}/A_T = 0.6$) f_{0i}(O)	f_{0i} (O)/ f_{0i}(I)
f_{01}	10.743	10.177	0.947
f_{02}	10.853	10.258	0.945
f_{03}	11.192	10.609	0.948
f_{04}	11.791	11.230	0.952
f_{05}	12.070	11.562	0.958
f_{06}	12.914	12.371	0.958
Frequencies (Hz)	Isotropic Model f_{0i}(I)	Orthotropic Model ($A_{rib}/A_T = 0.7$) f_{0i}(O)	f_{0i} (O)/ f_{0i}(I)
f_{01}	10.743	10.144	0.944
f_{02}	10.853	10.226	0.942
f_{03}	11.192	10.570	0.944
f_{04}	11.791	11.179	0.948
f_{05}	12.070	11.495	0.952
f_{06}	12.914	12.299	0.952
Frequencies (Hz)	Isotropic Model f_{0i}(I)	Orthotropic Model ($A_{rib}/A_T = 0.8$) f_{0i}(O)	f_{0i} (O)/ f_{0i}(I)
f_{01}	10.743	10.106	0.941
f_{02}	10.853	10.190	0.939
f_{03}	11.192	10.526	0.940
f_{04}	11.791	11.120	0.943
f_{05}	12.070	11.418	0.946
f_{06}	12.914	12.215	0.946
Frequencies (Hz)	Isotropic Model f_{0i}(I)	Orthotropic Model ($A_{rib}/A_T = 0.9$) f_{0i}(O)	f_{0i} (O)/ f_{0i}(I)
f_{01}	10.743	10.058	0.936
f_{02}	10.853	10.147	0.935
f_{03}	11.192	10.473	0.936
f_{04}	11.791	11.050	0.937
f_{05}	12.070	11.326	0.938
f_{06}	12.914	12.115	0.938

Finally the fundamental frequency obtained with the third model, see Tab. 8, was equal to f_{01}=12.05Hz was, as expected, higher than the experimental value, f_{01}=9.50Hz, [10] since all the model supports were considered rigid.

7.2 Boundary condition influence

Tabs. 3, 7, 8 and 9 indicate that fundamental frequencies were influenced by varying the model boundary conditions. When the first model natural frequencies, Tab. 3, are compared to the second and third models, Tabs. 7 and 8, it is possible to observe that as the beam-to-column joints stiffness is increased (the supports are transformed from simple to rigid) the natural frequencies also tended to increase. This conclusion is not valid for the fourth model, Tab. 9, since in this case, the natural frequencies were smaller than the previous three models, as presented in Tab. 3, 7 and 8.

The third model natural frequencies, Tab. 8, were higher than any of the other models. This is explained by the extremely stiffer beam-to-column joints adopted in modelling being much higher than the actual composite system frequencies.

These models also served to indicate that modelling the beam-to-column joint as simple connections, first model, or even rigid connections, second and third models, is not adequate confirming the joints semi-rigid response. The results of the present investigation suggest that future investigations should be centred on models that properly represent the actual beam-to-column joint stiffness like the fourth model. This is clearly seen by the fourth model fundamental frequency results, 9.3Hz that reached a good agreement with the experiments, 9.5Hz.

7.3 Composite system neutral axis location influence

The natural frequency results determined with the use of different models, Tabs. 2 to 6, confirmed the importance of the correct modelling of the composite system neutral axis location. As the composite system neutral axis location moves from the first to the fifth position (Fig. 6) the natural frequency values are significantly reduced.

Evidently, this fifth composite system neutral axis location was considered, in the present study, as a limit situation to establish the natural frequency variation when using the proposed models. In this case the natural frequency values are, as expected, much lower than any of the other studied cases, Tab. 6.

7.4 Steel deck geometry influence

Tab. 2 to 9 indicated that in all the cases investigated as the ratio AC/AT increases (meaning that the concrete area inside the steel deck ribs also increased when compared to the global AT) from AC/AT=50% up to AC/AT=90% the natural frequency values decrease. This conclusion is easily understood by the model mass increase associated with a negligible increase of structural system stiffness.

Table 4: First structural model: Third composite section neutral axis Position.

Frequencies (Hz)	Isotropic Model f_{0i}(I)	Orthotropic Model ($A_{rib}/A_T = 0.5$) f_{0i}(O)	f_{0i} (O)/ f_{0i}(I)
f_{01}	10.108	9.604	0.950
f_{02}	10.351	9.784	0.945
f_{03}	10.530	10.001	0.950
f_{04}	10.974	10.475	0.955
f_{05}	11.131	10.649	0.957
f_{06}	12.036	11.537	0.959
Frequencies (Hz)	Isotropic Model f_{0i}(I)	Orthotropic Model ($A_{rib}/A_T = 0.6$) f_{0i}(O)	f_{0i} (O)/ f_{0i}(I)
f_{01}	10.108	9.596	0.949
f_{02}	10.351	9.777	0.945
f_{03}	10.530	9.993	0.949
f_{04}	10.974	10.464	0.954
f_{05}	11.131	10.638	0.956
f_{06}	12.036	11.521	0.957
Frequencies (Hz)	Isotropic Model f_{0i}(I)	Orthotropic Model ($A_{rib}/A_T = 0.7$) f_{0i}(O)	f_{0i} (O)/ f_{0i}(I)
f_{01}	10.108	9.561	0.946
f_{02}	10.351	9.748	0.942
f_{03}	10.530	9.954	0.945
f_{04}	10.974	10.413	0.949
f_{05}	11.131	10.579	0.950
f_{06}	12.036	11.455	0.952
Frequencies (Hz)	Isotropic Model f_{0i}(I)	Orthotropic Model ($A_{rib}/A_T = 0.8$) f_{0i}(O)	f_{0i} (O)/ f_{0i}(I)
f_{01}	10.108	9.519	0.942
f_{02}	10.351	9.715	0.939
f_{03}	10.530	9.908	0.941
f_{04}	10.974	10.354	0.944
f_{05}	11.131	10.513	0.944
f_{06}	12.036	11.379	0.945
Frequencies (Hz)	Isotropic Model f_{0i}(I)	Orthotropic Model ($A_{rib}/A_T = 0.9$) f_{0i}(O)	f_{0i} (O)/ f_{0i}(I)
f_{01}	10.108	9.467	0.937
f_{02}	10.351	9.675	0.935
f_{03}	10.530	9.854	0.936
f_{04}	10.974	10.284	0.937
f_{05}	11.131	10.436	0.938
f_{06}	12.036	11.288	0.938

Table 5: First structural model: Fourth composite section neutral axis position.

Frequencies (Hz)	Isotropic Model f_{0i}(I)	Orthotropic Model ($A_{rib}/A_T = 0.5$) f_{0i}(O)	f_{0i} (O)/ f_{0i}(I)
f_{01}	9.655	9.185	0.951
f_{02}	9.998	9.465	0.947
f_{03}	10.061	9.570	0.951
f_{04}	10.437	9.971	0.955
f_{05}	10.595	10.104	0.954
f_{06}	11.478	10.997	0.958
Frequencies (Hz)	Isotropic Model f_{0i}(I)	Orthotropic Model ($A_{rib}/A_T = 0.6$) f_{0i}(O)	f_{0i} (O)/ f_{0i}(I)
f_{01}	9.655	9.178	0.951
f_{02}	9.998	9.458	0.946
f_{03}	10.061	9.562	0.950
f_{04}	10.437	9.960	0.954
f_{05}	10.595	10.094	0.953
f_{06}	11.478	10.982	0.957
Frequencies (Hz)	Isotropic Model f_{0i}(I)	Orthotropic Model ($A_{rib}/A_T = 0.7$) f_{0i}(O)	f_{0i} (O)/ f_{0i}(I)
f_{01}	9.655	9.141	0.947
f_{02}	9.998	9.428	0.943
f_{03}	10.061	9.519	0.946
f_{04}	10.437	9.908	0.949
f_{05}	10.595	10.044	0.948
f_{06}	11.478	10.919	0.951
Frequencies (Hz)	Isotropic Model f_{0i}(I)	Orthotropic Model ($A_{rib}/A_T = 0.8$) f_{0i}(O)	f_{0i} (O)/ f_{0i}(I)
f_{01}	9.655	9.097	0.942
f_{02}	9.998	9.393	0.939
f_{03}	10.061	9.471	0.941
f_{04}	10.437	9.850	0.944
f_{05}	10.595	9.989	0.943
f_{06}	11.478	10.847	0.945
Frequencies (Hz)	Isotropic Model f_{0i}(I)	Orthotropic Model ($A_{rib}/A_T = 0.9$) f_{0i}(O)	f_{0i} (O)/ f_{0i}(I)
f_{01}	9.655	9.045	0.937
f_{02}	9.998	9.350	0.935
f_{03}	10.061	9.415	0.936
f_{04}	10.437	9.782	0.937
f_{05}	10.595	9.925	0.937
f_{06}	11.478	10.762	0.938

Table 6: First structural model: Fifth composite section neutral axis position.

Frequencies (Hz)	Isotropic Model f_{0i}(I)	Orthotropic Model ($A_{rib}/A_T = 0.5$) f_{0i}(O)	f_{0i} (O)/ f_{0i}(I)
f_{01}	6.021	5.665	0.941
f_{02}	6.114	5.751	0.941
f_{03}	6.343	6.008	0.947
f_{04}	6.724	6.426	0.956
f_{05}	6.949	6.703	0.965
f_{06}	8.972	8.567	0.955
Frequencies (Hz)	Isotropic Model f_{0i}(I)	Orthotropic Model ($A_{rib}/A_T = 0.6$) f_{0i}(O)	f_{0i} (O)/ f_{0i}(I)
f_{01}	6.021	5.663	0.941
f_{02}	6.114	5.748	0.940
f_{03}	6.343	6.004	0.946
f_{04}	6.724	6.419	0.955
f_{05}	6.949	6.694	0.963
f_{06}	8.972	8.555	0.954
Frequencies (Hz)	Isotropic Model f_{0i}(I)	Orthotropic Model ($A_{rib}/A_T = 0.7$) f_{0i}(O)	f_{0i} (O)/ f_{0i}(I)
f_{01}	6.021	5.651	0.939
f_{02}	6.114	5.736	0.938
f_{03}	6.343	5.982	0.943
f_{04}	6.724	6.383	0.949
f_{05}	6.949	6.639	0.955
f_{06}	8.972	8.508	0.948
Frequencies (Hz)	Isotropic Model f_{0i}(I)	Orthotropic Model ($A_{rib}/A_T = 0.8$) f_{0i}(O)	f_{0i} (O)/ f_{0i}(I)
f_{01}	6.021	5.638	0.936
f_{02}	6.114	5.723	0.936
f_{03}	6.343	5.958	0.939
f_{04}	6.724	6.343	0.943
f_{05}	6.949	6.580	0.947
f_{06}	8.972	8.455	0.942
Frequencies (Hz)	Isotropic Model f_{0i}(I)	Orthotropic Model ($A_{rib}/A_T = 0.9$) f_{0i}(O)	f_{0i} (O)/ f_{0i}(I)
f_{01}	6.021	5.623	0.934
f_{02}	6.114	5.708	0.934
f_{03}	6.343	5.932	0.935
f_{04}	6.724	6.293	0.936
f_{05}	6.949	6.518	0.938
f_{06}	8.972	8.397	0.936

Table 7: Second structural model.

Frequencies (Hz)	Isotropic Model f_{0i}(I)	Orthotropic Model ($A_{rib}/A_T = 0.5$) f_{0i}(O)	f_{0i} (O)/ f_{0i}(I)
f_{01}	10.842	10.241	0.945
f_{02}	10.930	10.346	0.947
f_{03}	11.218	10.648	0.949
f_{04}	11.825	11.277	0.954
f_{05}	12.433	11.920	0.959
f_{06}	14.249	13.680	0.960
Frequencies (Hz)	Isotropic Model f_{0i}(I)	Orthotropic Model ($A_{rib}/A_T = 0.6$) f_{0i}(O)	f_{0i} (O)/ f_{0i}(I)
f_{01}	10.842	10.235	0.944
f_{02}	10.930	10.339	0.946
f_{03}	11.218	10.639	0.948
f_{04}	11.825	11.267	0.953
f_{05}	12.433	11.907	0.958
f_{06}	14.249	13.661	0.959
Frequencies (Hz)	Isotropic Model f_{0i}(I)	Orthotropic Model ($A_{rib}/A_T = 0.7$) f_{0i}(O)	f_{0i} (O)/ f_{0i}(I)
f_{01}	10.842	10.206	0.941
f_{02}	10.930	10.308	0.943
f_{03}	11.218	10.600	0.945
f_{04}	11.825	11.214	0.948
f_{05}	12.433	11.839	0.952
f_{06}	14.249	13.578	0.953
Frequencies (Hz)	Isotropic Model f_{0i}(I)	Orthotropic Model ($A_{rib}/A_T = 0.8$) f_{0i}(O)	f_{0i} (O)/ f_{0i}(I)
f_{01}	10.842	10.173	0.938
f_{02}	10.930	10.271	0.940
f_{03}	11.218	10.554	0.941
f_{04}	11.825	11.153	0.943
f_{05}	12.433	11.760	0.946
f_{06}	14.249	13.482	0.946
Frequencies (Hz)	Isotropic Model f_{0i}(I)	Orthotropic Model ($A_{rib}/A_T = 0.9$) f_{0i}(O)	f_{0i} (O)/ f_{0i}(I)
f_{01}	10.842	10.134	0.935
f_{02}	10.930	10.227	0.936
f_{03}	11.218	10.499	0.936
f_{04}	11.825	11.081	0.937
f_{05}	12.433	11.666	0.938
f_{06}	14.249	13.366	0.938

Another important conclusion could be made concerning the relation between the orthotropic $f_{0i}(O)$, and isotropic $f_{0i}(I)$, models natural frequencies. In all considered cases, Tabs. 2 to 9, the ratio $f_{0i}(O)/f_{0i}(I)$, only varied from 94% up to 96% of the isotropic model natural frequencies. This interesting issue indicates, for the analysed structural system, that structural designers do not necessarily need to consider an orthotropic model to obtain the composite system natural frequencies, Tabs. 2 to 9.

7.5 Vibration mode analysis

The present paper only presents the six first composite system vibration modes using isotropic and orthotropic solutions (with an associated A_{rib}/A_T ratio equal to 0.5) for the first, second and fourth proposed models, Figs. 9 to 14.

The vibration modes for the various investigated models of the orthotropic system proved to be qualitatively similar to the vibration modes associated to the isotropic solutions. However, as the boundary conditions change, from model to model, the composite system vibration mode configurations are altered. This fact also corroborates the importance of properly modelling beam-to-column joints in current design practice.

8 Final remarks

This paper presented the evaluation of the structural dynamical behaviour of composite floors with profiled steel decks. The proposed analysis methodology investigated the linear dynamic behaviour of a 14m by 43.7m building floor made of a composite slab system with welded wide flange (WWF) beams and a profiled steel deck.

One of the main objectives of this investigation was to evaluate the orthotrophy effect on the dynamic response of these composite floors. Four finite element models were developed, using the ANSYS program [1] to investigate the modelling refinement level on the dynamical behaviour of the analysed structural system.

The finite element models were developed and refined according to comparisons made between the numerical and experimental fundamental frequency results. The results obtained along the present investigation indicated that the effect of some design parameters like: boundary conditions, composite system neutral axis location, steel deck geometry and the actual stiffness provided by the beam to-columns joints can significantly affect the composite system natural frequencies.

The investigated structural system presented natural frequencies values that were not significantly modified when orthotropic or isotropic models were considered. This fact can be explained due to the particular structural system geometry in which one of the slab dimensions is almost three times the other. In this particular case, the orthotrophy effects became significantly reduced causing only slight differences on the composite floor natural frequencies values when compared to the isotropic modelling.

Table 8: Third structural model.

Frequencies (Hz)	Isotropic Model f_{0i}(I)	Orthotropic Model ($A_{rib}/A_T = 0.5$) f_{0i}(O)	f_{0i} (O)/ f_{0i}(I)
f_{01}	12.573	12.054	0.959
f_{02}	12.924	12.384	0.958
f_{03}	13.547	12.983	0.958
f_{04}	13.807	13.212	0.957
f_{05}	15.539	14.893	0.958
f_{06}	16.643	16.013	0.962
Frequencies (Hz)	Isotropic Model f_{0i}(I)	Orthotropic Model ($A_{rib}/A_T = 0.6$) f_{0i}(O)	f_{0i} (O)/ f_{0i}(I)
f_{01}	12.573	12.036	0.957
f_{02}	12.924	12.366	0.957
f_{03}	13.547	12.964	0.957
f_{04}	13.807	13.195	0.956
f_{05}	15.539	14.874	0.957
f_{06}	16.643	15.989	0.961
Frequencies (Hz)	Isotropic Model f_{0i}(I)	Orthotropic Model ($A_{rib}/A_T = 0.7$) f_{0i}(O)	f_{0i} (O)/ f_{0i}(I)
f_{01}	12.573	11.968	0.952
f_{02}	12.924	12.297	0.951
f_{03}	13.547	12.892	0.952
f_{04}	13.807	13.123	0.950
f_{05}	15.539	14.790	0.952
f_{06}	16.643	15.885	0.954
Frequencies (Hz)	Isotropic Model f_{0i}(I)	Orthotropic Model ($A_{rib}/A_T = 0.8$) f_{0i}(O)	f_{0i} (O)/ f_{0i}(I)
f_{01}	12.573	11.889	0.946
f_{02}	12.924	12.217	0.945
f_{03}	13.547	12.809	0.946
f_{04}	13.807	13.040	0.944
f_{05}	15.539	14.692	0.945
f_{06}	16.643	15.764	0.947
Frequencies (Hz)	Isotropic Model f_{0i}(I)	Orthotropic Model ($A_{rib}/A_T = 0.9$) f_{0i}(O)	f_{0i} (O)/ f_{0i}(I)
f_{01}	12.573	11.797	0.938
f_{02}	12.924	12.123	0.938
f_{03}	13.547	12.712	0.938
f_{04}	13.807	12.943	0.937
f_{05}	15.539	14.575	0.938
f_{06}	16.643	15.619	0.938

Table 9: Fourth structural model.

Frequencies (Hz)	Isotropic Model f_{0i}(I)	Orthotropic Model ($A_{rib}/A_T = 0.5$) f_{0i}(O)	f_{0i} (O)/ f_{0i}(I)
f_{01}	9.805	9.305	0.948
f_{02}	10.096	9.562	0.947
f_{03}	10.566	10.032	0.949
f_{04}	11.515	10.973	0.953
f_{05}	12.455	11.957	0.960
f_{06}	13.691	13.101	0.957
Frequencies (Hz)	Isotropic Model f_{0i}(I)	Orthotropic Model ($A_{rib}/A_T = 0.5$) f_{0i}(O)	f_{0i} (O)/ f_{0i}(I)
f_{01}	9.805	9.285	0.947
f_{02}	10.096	9.554	0.946
f_{03}	10.566	10.023	0.949
f_{04}	11.515	10.962	0.952
f_{05}	12.455	11.943	0.959
f_{06}	13.691	13.085	0.956
Frequencies (Hz)	Isotropic Model f_{0i}(I)	Orthotropic Model ($A_{rib}/A_T = 0.5$) f_{0i}(O)	f_{0i} (O)/ f_{0i}(I)
f_{01}	9.805	9.256	0.944
f_{02}	10.096	9.527	0.944
f_{03}	10.566	9.988	0.945
f_{04}	11.515	10.915	0.948
f_{05}	12.455	11.875	0.953
f_{06}	13.691	13.015	0.951
Frequencies (Hz)	Isotropic Model f_{0i}(I)	Orthotropic Model ($A_{rib}/A_T = 0.5$) f_{0i}(O)	f_{0i} (O)/ f_{0i}(I)
f_{01}	9.805	9.222	0.941
f_{02}	10.096	9.494	0.940
f_{03}	10.566	9.947	0.941
f_{04}	11.515	10.860	0.943
f_{05}	12.455	11.794	0.947
f_{06}	13.691	12.934	0.945
Frequencies (Hz)	Isotropic Model f_{0i}(I)	Orthotropic Model ($A_{rib}/A_T = 0.5$) f_{0i}(O)	f_{0i} (O)/ f_{0i}(I)
f_{01}	9.805	9.180	0.936
f_{02}	10.096	9.453	0.936
f_{03}	10.566	9.897	0.937
f_{04}	11.515	10.794	0.937
f_{05}	12.455	11.696	0.939
f_{06}	13.691	12.836	0.938

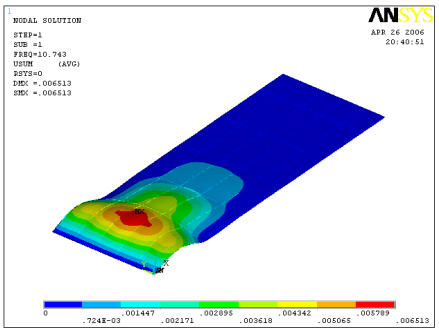

(a) Vibration mode associated to the 1^{st} natural frequency: f_{01}=10.743 Hz.

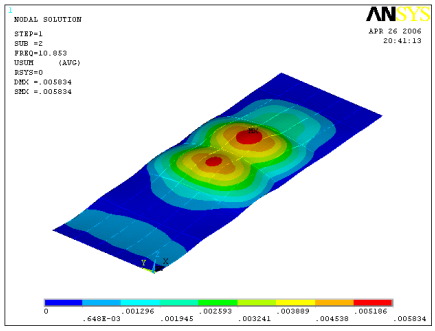

(b) Vibration mode associated to the 2^{nd} natural frequency: f_{02}=10.853 Hz.

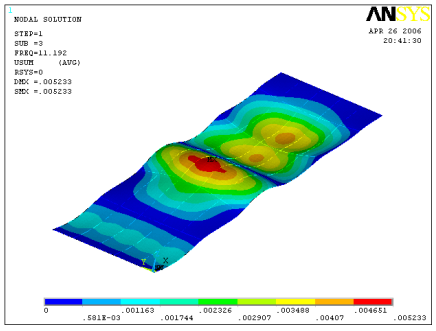

(c) Vibration mode associated to the 3^{rd} natural frequency: f_{03}=11.192 Hz.

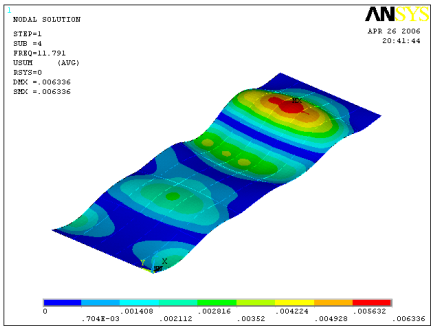

(d) Vibration mode associated to the 4^{th} natural frequency: f_{04}=11.791 Hz.

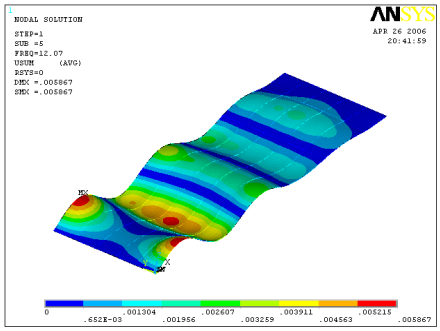

(e) Vibration mode associated to the 5^{th} natural frequency: f_{05}=12.070 Hz.

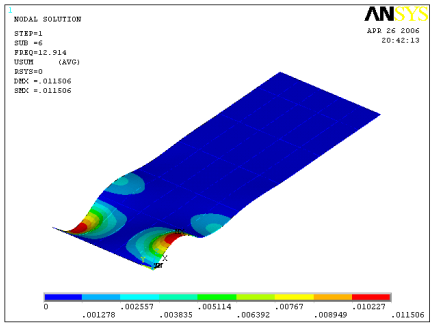

(f) Vibration mode associated to the 6^{th} natural frequency: f_{06}=12.914 Hz.

Figure 9: Vibration modes related to the first isotropic structural model.

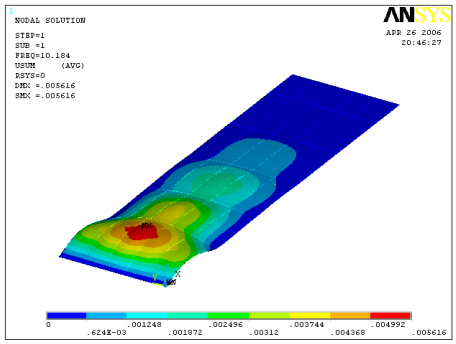

(a) Vibration mode associated to the 1^{st} natural frequency: f_{01}=10.184 Hz.

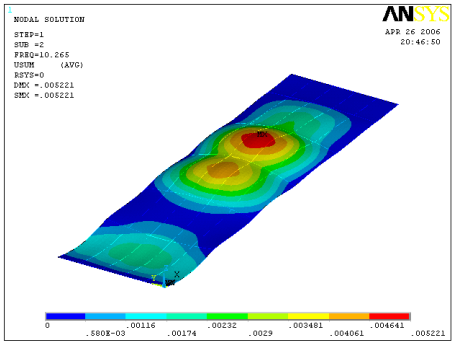

(b) Vibration mode associated to the 2^{nd} natural frequency: f_{02}=10.265 Hz.

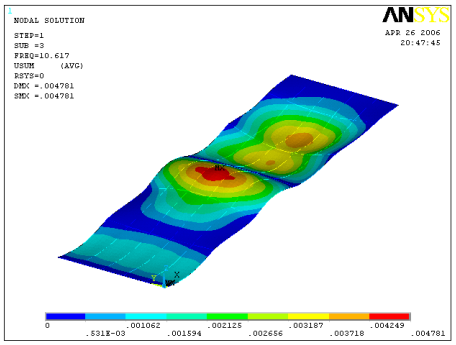

(c) Vibration mode associated to the 3^{rd} natural frequency: f_{03}=10.617 Hz.

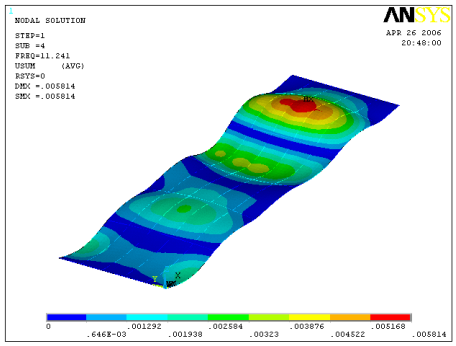

(d) Vibration mode associated to the 4^{th} natural frequency: f_{04}=11.241 Hz.

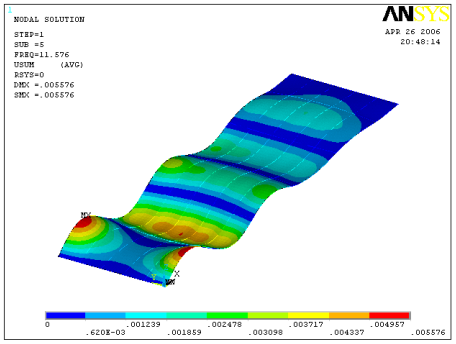

(e) Vibration mode associated to the 5^{th} natural frequency: f_{05}= 11.576 Hz.

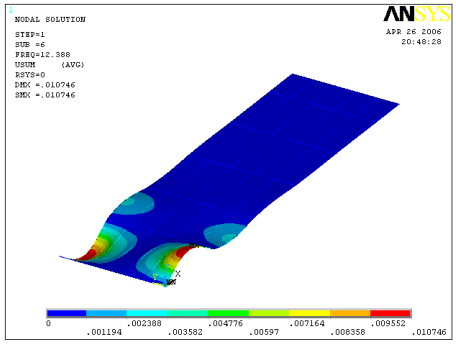

(f) Vibration mode associated to the 6^{th} natural frequency: f_{06}=12.388 Hz.

Figure 10: Vibration modes related to the first orthotropic model (A_{rib}/A_T = 0.50).

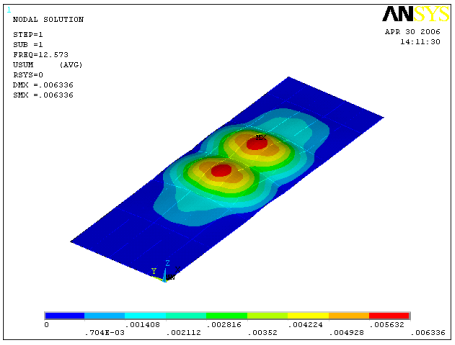

(a) Vibration mode associated to the 1^{st} natural frequency: f_{01}=12.573 Hz.

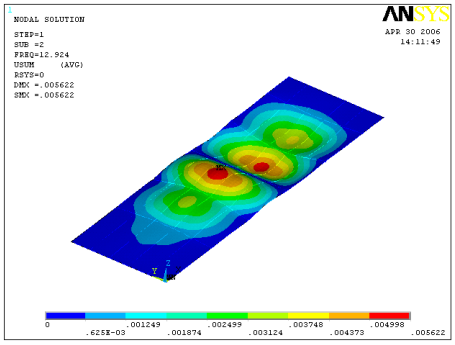

(b) Vibration mode associated to the 2^{nd} natural frequency: f_{02}=12.924 Hz.

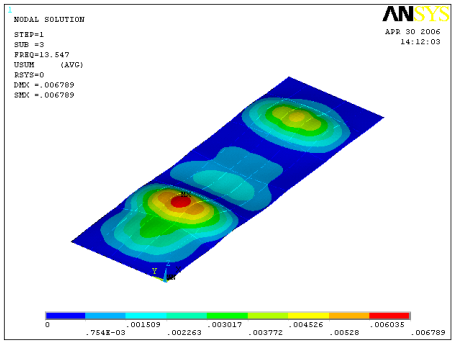

(c) Vibration mode associated to the 3^{rd} natural frequency: f_{03}=13.547 Hz.

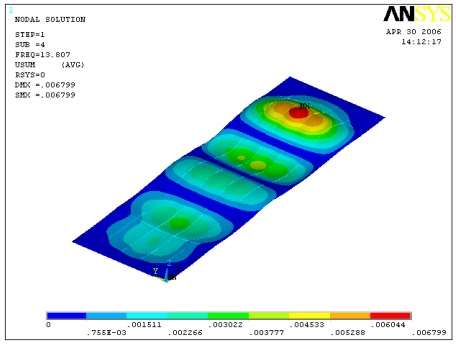

(d) Vibration mode associated to the 4^{th} natural frequency: f_{04}=13.807 Hz.

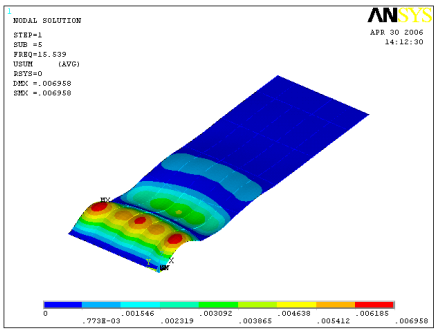

(e) Vibration mode associated to the 5^{th} natural frequency: f_{05}=15.539 Hz.

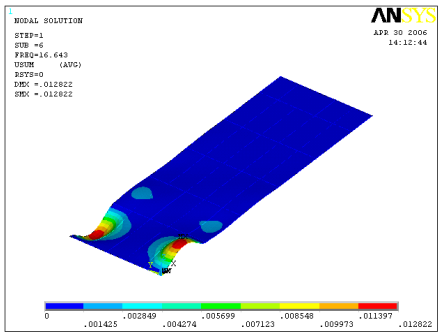

(f) Vibration mode associated to the 6^{th} natural frequency: f_{06}=16.643 Hz.

Figure 11: Vibration modes related to the second isotropic structural model.

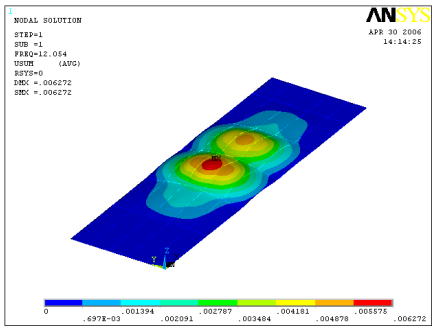

(a) Vibration mode associated to the 1^{st} natural frequency: f_{01}=12.054 Hz.

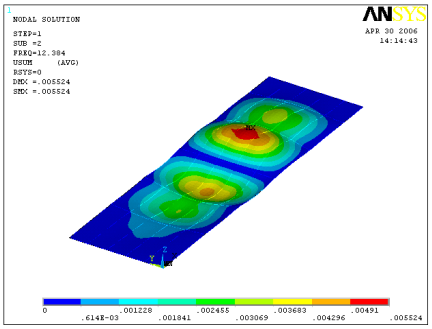

(b) Vibration mode associated to the 2^{nd} natural frequency: f_{02}=12.384 Hz.

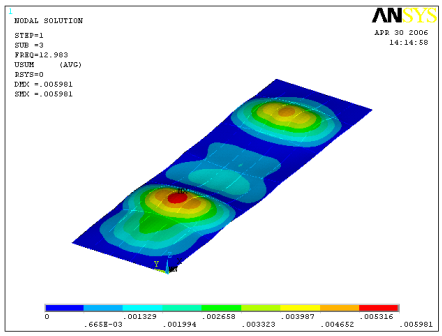

(c) Vibration mode associated to the 3^{rd} natural frequency: f_{03}=12.983 Hz.

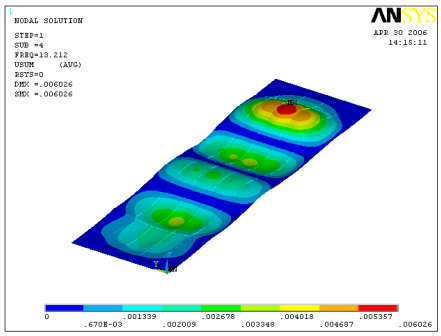

(d) Vibration mode associated to the 4^{th} natural frequency: f_{04}=13.212 Hz.

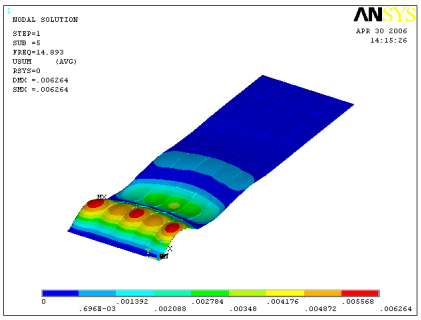

(e) Vibration mode associated to the 5^{th} natural frequency: f_{05}=14.893 Hz.

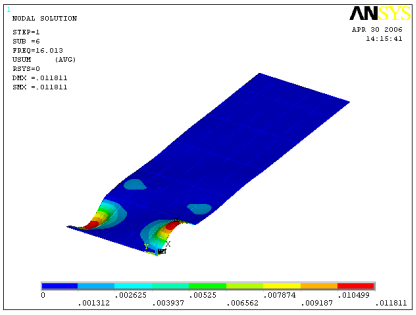

(f) Vibration mode associated to the 6^{th} natural frequency: f_{06}=16.013 Hz.

Figure 12: Vibration modes related to the second orthotropic model ($A_{rib}/A_T = 0.50$).

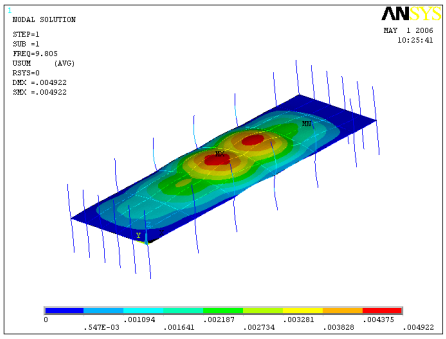

(a) Vibration mode associated to the 1^{st} natural frequency: f_{01}=9.805 Hz.

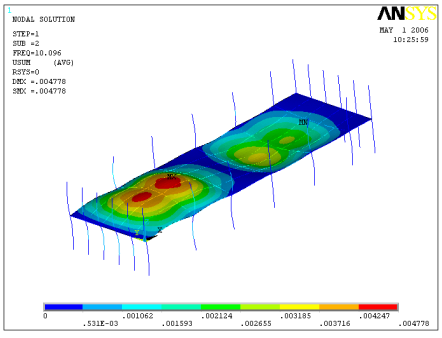

(b) Vibration mode associated to the 2^{nd} natural frequency: f_{02}= 10.096 Hz.

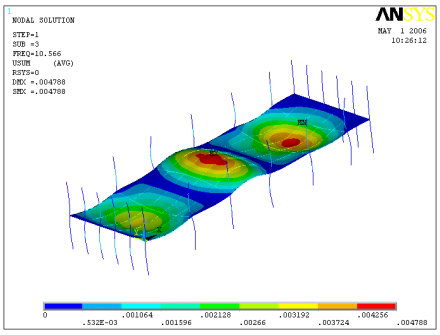

(c) Vibration mode associated to the 3^{rd} natural frequency: f_{03}=10.566 Hz.

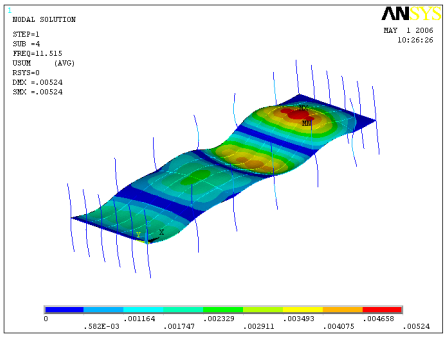

(d) Vibration mode associated to the 4^{th} natural frequency: f_{04}=11.515 Hz.

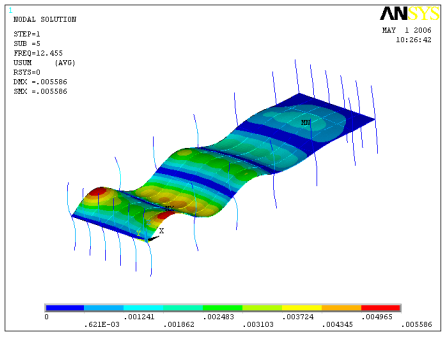

(e) Vibration mode associated to the 5^{th} natural frequency: f_{05}=12.455 Hz.

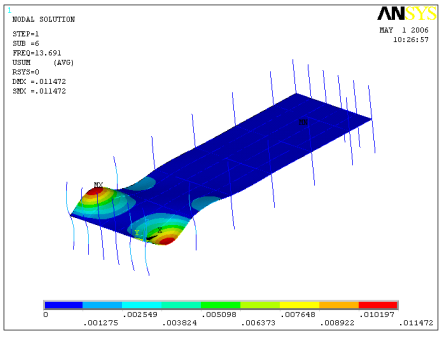

(f) Vibration mode associated to the 6^{th} natural frequency: f_{06}=13.691 Hz.

Figure 13: Vibration modes related to the fourth isotropic structural model.

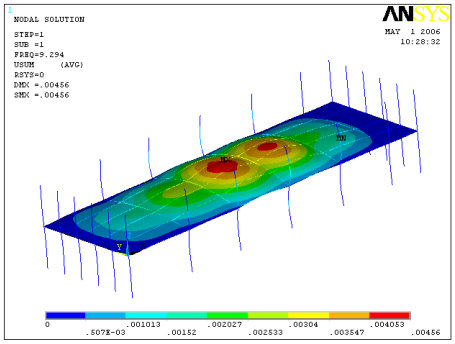

(a) Vibration mode associated to the 1^{st} natural frequency: f_{01}=9.294 Hz.

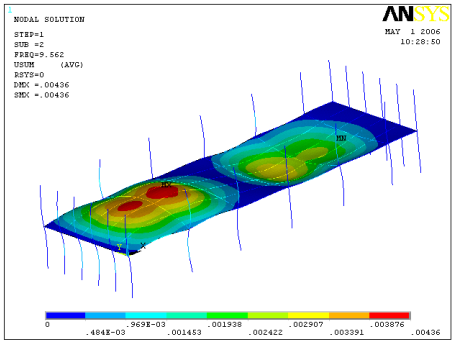

(b) Vibration mode associated to the 2^{nd} natural frequency: f_{02}=9.562 Hz.

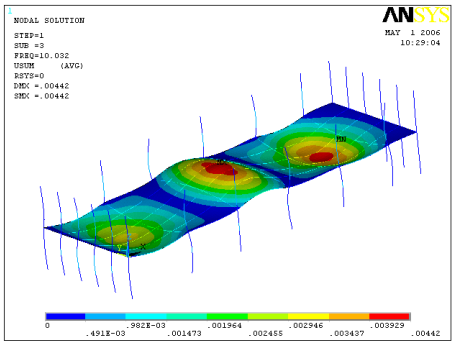

(c) Vibration mode associated to the 3^{rd} natural frequency: f_{03}=10.032 Hz.

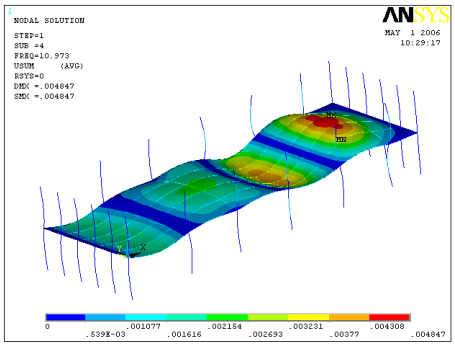

(d) Vibration mode associated to the 4^{th} natural frequency: f_{04}=10.973 Hz.

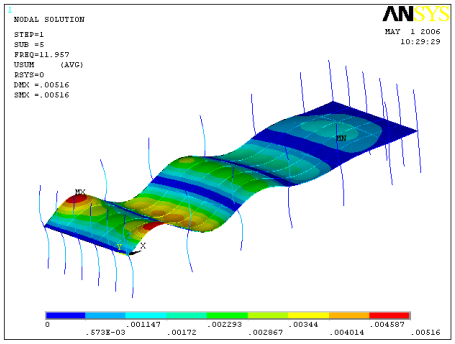

(e) Vibration mode associated to the 5^{th} natural frequency: f_{05}=11.957 Hz.

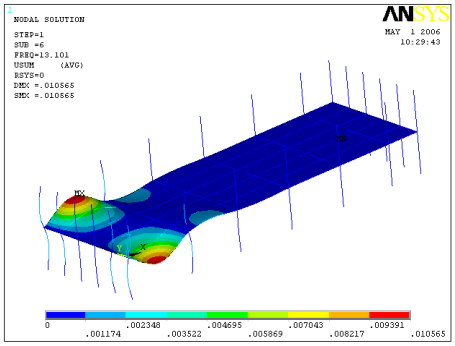

(f) Vibration mode associated to the 6^{th} natural frequency: f_{06}=13.101 Hz.

Figure 14: Vibration modes related to the fourth orthotropic model (A_{rib}/A_T = 0.50).

The adopted steel deck profile was not sufficient to induce a significant orthotrophy characteristic to the investigated composite slab system. This was reflected on the vibration modes for the various investigated models of the orthotropic system that were qualitatively similar to the vibration modes associated to the isotropic solutions. However, as soon as the boundary conditions change, the composite system vibration modes configurations are modified.

The results and conclusions of the present study suggest the continuation of an extensive parametric study considering design parameters like the beam-to-column joint modelling, primary and secondary girder spans, geometrical characteristics of the steel sections and the concrete slab and alternative structural systems.

Acknowledgments

The authors would like to thank the financial support provided by the National and State Scientific and Technological Agencies: CNPq, CAPES and FAPERJ.

References

[1] Inc. ANSYS, Swanson analysis systems. *Basic analysis procedures*. P.O. Box 65, Johnson Road, Houston, PA, 15342-0065, 2 edition, 1998. version 5.5.

[2] H. Bachmann and W. Ammann. Vibrations in structures induced by man and machines. *IABSE Structural Engineering Document 3E, International Association for Bridges and Structural Engineering*, 1987. ISBN 3-85748-052-X.

[3] Y. Chen. Finite element analysis for walking vibration problems for composite precast building floors using adina: modelling; simulation, and comparison. *Computers & Structures*, 72:109–126, 1999.

[4] J. G. S. da Silva, F. J. da C. P. Soeiro, P. C. G. da S. Vellasco, Andrade S. A. L de, and R. N. Werneck. Dynamical analysis of composite steel decks floors subjected to rhythmic load actions. In *8^{th} International Conference on Civil and Structural Engineering Computing, CIVIL COMP-2001*, Áustria, 2001. CD-ROM, 16 pages.

[5] J. G. S. da Silva, F. J. da C. P. Soeiro, P. C. G. da S. Vellasco, Andrade S. A. L de, and R. N. Werneck. Dynamical response of steel deck composite slabs with geometric orthotrophy subjected to human rhythmic activities. In *6^{th} International Conference on Computational Structures Technology, CST 2002*, Praga, 2002. CD-ROM, 17 pages.

[6] A. V. de A. Mello. Vibrações em pisos de edificações induzidas por atividades humanas. Master's thesis, Programa de Pós-Graduação em Engenharia Civil – PGECIV, Universidade do Estado do Rio de Janeiro, UERJ, Rio de Janeiro, Brasil, 2005. (in Portuguese).

[7] A. V. de A. Mello, J. G. S. da Silva, and L. R. O. de Lima. Análise de pisos de edificações submetidos à ações dinâmicas provenientes do caminhar humano. *CILAMCE XXVI, Iberian Latin American Congress on Computational Methods in Engineering*, 2005. CD-ROM, 14 pages (in Portuguese).

[8] T. M. Murray, D. E. Allen, and E. E. Ungar. Floor vibrations due to human activity. *Steel Design Guide Series, 11th Steel Design Guide Series, American Institute of Steel Construction, AISC*, 1997.

[9] D. J. Oehlers and M. A. Bradford. *Elementary Behaviour of Composite Steel & Concrete Structural Members*. Butterworth-Heinemann, London, UK, 1999.

[10] M. A. M. Vecci, R. H. Fakury, and P. V. P. Mendonça. Análise de vibrações de pisos submetidos a excitações rítmicas. aplicação de critérios para conforto em edificações. In *Encontro Nacional de Conforto no Ambiente Construído. III Encontro Latino-Amercano de Conforto no Ambiente Construído. Brasil*, pages 1–6. (in Portuguese), 1999.